Engineering Fracture Mechanics 288 (2023) 109352

Contents lists available at ScienceDirect

Engineering Fracture Mechanics

journal homepage: www.elsevier.com/locate/engfracmech

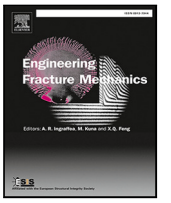

Rate-dependency analysis of mode I delamination by means of different data reduction strategies for the GDCB test method

S.A. Medina [a,*], E.V. González [a,*], N. Blanco [a], P. Maimí [a], J. Pernas-Sánchez [b], J.A. Artero-Guerrero [b], P. Hahn [c], M. May [c], E. de Blanpré [d], V. Jacques [d]

[a] AMADE - Analysis and Advanced Materials for Structural Design, Polytechnic school, Universitat de Girona, Carrer de Maria Aurèlia Capmany i Farnés, 61, Girona, Spain
[b] Department of Continuum Mechanics and Structural Analysis, Universidad Carlos III de Madrid, Leganés, Madrid, Spain
[c] Fraunhofer Institute for High-Speed Dynamics, Ernst-Mach-Institute, EMI, Ernst-Zermelo-Straße 4, Freiburg, Germany
[d] Dassault Aviation, 78 Quai Marcel Dassault, Saint-Cloud, France

ARTICLE INFO

Keywords:
Rate-dependency
Fracture toughness
Data reduction method
Loading-rate
Dynamic effects

ABSTRACT

The loading-rate mechanical response of the mode I delamination in composites and adhesively bonded joints was investigated. The tests were carried out using a recently developed Guided Double Cantilever Beam test method. Three different data reduction methods were proposed and assessed: a displacement-based formulation, a near-crack-tip displacement formulation, and a numerical assessment using the Virtual Crack-Closure Technique method. The methods account for the dynamic effects which may be present. While small differences between the three different methods can be seen, no rate-dependency higher than the uncertainty for the materials and the loading rates considered have been evidenced.

1. Introduction

The use of composites and adhesive joining of composites continues to attract interest in aerospace, automotive and military applications. Even so, a mature knowledge of the properties and behaviour under high loading rates, especially in the field of fracture behaviour, is still required. Despite being a matter of research during the last decades, the rate-dependency of the fracture toughness of Fibre-Reinforced Plastics (FRPs) and adhesive joints in FRPs still needs to be well understood and characterised to improve the reliability of numerical predictions in dynamic events.

Although there is a lack of consensus in the literature as to which test method for the dynamic characterisation of the fracture energy should be used, it is clear that the dynamic effect analysis is highly affected by the data reduction method used [1,2]. The parameters involved in the data reduction, such as load, strain, displacement or crack length, remain critical when analysing the rate-dependency of the material. Most data reduction methods for deriving the fracture toughness were developed with quasi-static observations in mind. However, it has been shown that the type of test set-up, for instance, using high-speed cameras, can influence the accuracy of the relevant measurements of the parameters involved in the data analysis [3,4].

The data reduction methods for mode I tests under quasi-static conditions are normally based on Linear Elastic Fracture Mechanics (LEFM), as in the case of the international standards ISO [5], widely used to characterise the propagation of interlaminar cracks in fibre-reinforced composites, and ISO [6] used to determine the fracture energy of adhesively bonded joints. According to Blackman et al. [7], different correction factors must be included when determining the mode I interlaminar fracture energy, G_{Ic}, for the Double Cantilever Beam (DCB) test.

* Corresponding author.
E-mail addresses: sergio.medina@udg.edu (S.A. Medina), emilio.gonzalez@udg.edu (E.V. González).

https://doi.org/10.1016/j.engfracmech.2023.109352
Received 29 January 2023; Received in revised form 28 April 2023; Accepted 17 May 2023
Available online 23 May 2023

Nomenclature

a	Crack length
a_e	Effective crack length
b	Specimen width
c_o	Longitudinal wave propagation velocity in the material
C	GDCB compliance
E	Flexural modulus of the laminate or the adherents
G_I	Mode I energy release rate
G_{Ic}	Mode I interlaminar fracture energy
h	Half of the specimen thickness
I	Second moment of area of the cross section
m	Lumped mass at the free end of a cantilever beam
M	Equivalent moment
n	Grade of the polynomial expressions
P	Load
R_y	Reaction force for the VCCT
$u(x)$	Opening displacement of one arm at a distance x
$\dot{u}(x)$	Opening displacement rate of one arm at a distance x
U_k	Kinetic energy
x	Longitudinal distance from the crack tip to the loading point
δ	Opening displacement at the loading point
$\dot{\delta}$	Opening displacement rate at the loading point
Δa	Crack length extension for the VCCT
Δu_y	Separation displacement for the VCCT
ρ	Density of the material
$\phi(x)$	Rotation of the arms near the crack tip
φ^{-1}	Flexural rigidity of the beam
χ	Constant for the effective crack length correction factor
$\omega(x)$	Opening displacement of the arms near the crack tip

Acronyms

CBT	Corrected Beam Theory
DCB	Double Cantilever Beam
FE	Finite Element
FRPs	Fibre-Reinforced Plastics
GDCB	Guided Double Cantilever Beam
LEFM	Linear Elastic Fracture Mechanics
MWIF	Modified Wedge-Insert Fracture
QS	Quasi-static
SCB	Side-Clamped Beam
SHPB	Split Hopkinson Pressure Bar
VCCT	Virtual Crack-Closure Technique

As LEFM is a very reliable method for quasi-static analyses, different authors have used the same approach for dynamic tests as well. However, this approach does not account for the dynamic effects present during high loading rate tests and is, consequently, one of the major reasons for such differing results present in the literature. It has been shown that the data reduction method used is a key factor to correctly account for the dynamic effects during a dynamic characterisation of the fracture energy [1,2]. Interpreting results from dynamic fracture experiments is complex because of three factors: (a) the inertia of the specimen and additional elements bonded to it, (b) the time dependence of the material, and (c) the reflected stress waves that alter the stress state at the crack tip. Since the quasi-static data reductions are not reliable for most of the cases, a deeper analysis of these dynamic effects is required.

An important point about the experimental analysis of high-rate tests, in particular with inertia effects, is that the applied load cannot be measured accurately because of signal oscillations [1,8,9]. For that reason, Blackman et al. [7] developed a load-independent (displacement-based) analysis for the dynamic DCB fracture toughness. In a first step of their research, they used a

simple displacement-based LEFM analysis which does not require a direct knowledge of the load. Following this, an energy analysis was developed to account for the dynamic effects for the same DCB test [1,8]. They proposed two cases with which to analyse the dynamic fracture toughness where the kinetic energy in the moving specimen arms was significant when compared to the fracture energy: case 1, unstable crack growth (prior to crack propagation when the crack speed is zero in stick slip events); and case 2, stable crack growth (for steady-state crack propagation where there is a velocity contribution from the crack motion).

Despite this dynamic analysis having been proposed several years ago, most authors still use the quasi-static approach for G_{Ic} ignoring the dynamic effects [10–14]. In the work of Isakov et al. [15], it is proved that using a quasi-static framework is valid for their test and loading rates. They showed that the contribution of the kinetic energy can be assumed to be minimal for all the tested loading rates and is only important for loading rates above 30 m/s. Only a few works present in the literature include the kinetic effects in the analysis. For example, Thorsson et al. [16] included the kinetic energy contribution to their Modified Wedge-Insert Fracture (MWIF) method using simple beam theory.

Some other analyses have been performed using different strategies and theories to account for dynamic mode I fracture toughness. Riezzo et al. [17] performed dynamic wedge-insert tests using a thermal–mechanical physical system (based on a hydraulic system) to obtain the interlaminar fracture toughness in composite laminates. They used a quasi-static calibrated compliance curve with a load-dependent analysis to obtain the fracture energy in dynamic tests. Because wedge-insert tests involve friction between the wedge and the cracked surfaces of the specimen, the load was measured indirectly by means of strain gauges attached to the specimen. Lißner et al. [18] used the J-integral theory to measure the fracture energy of adhesive interfaces in a Split Hopkinson Pressure Bar (SHPB). However, assuming that the equations derived from quasi-static equilibrium are valid for high-rate analysis, no dynamic effect was considered.

A relevant concluding remark is that although different analytical approaches have been used in the literature, there is no clear evidence on how the dynamic effects affect the characterisation of the mode I fracture toughness in FRPs and adhesively bonded joints.

This paper presents a study of different data reduction strategies for the Guided Double Cantilever Beam (GDCB) test method proposed by Medina et al. [19], to measure the mode I fracture toughness in composites and adhesive joints under different loading rates. Three different data reduction methods have been assessed: a displacement-based formulation taking into account the dynamic contribution through the kinetic energy, a near-crack-tip displacement formulation, and a numerical assessment based on the experimental specimen arms displacements and using the Virtual Crack-Closure Technique (VCCT) method. A validation of the data reduction strategies was conducted by comparing the quasi-static mode I fracture toughness obtained with the GDCB method and the standardised ISO [5,6] methods. A test campaign from quasi-static up to high loading rates (maximum opening velocity of 30 m/s), was carried out to show the performance of the data reduction methods at the different loading rates.

The GDCB, as shown in Fig. 1, is a test set-up developed in-house to characterise dynamic mode I fracture toughness. As seen in Fig. 1, the device introduces the load through a V-shape guidance system that allows a constant velocity (after the acceleration period of the machine) to be reached. The tool also includes a pair of hinges clamped to the arms of the specimen that transfer the load/displacement from the main part of the tool, along with a simple, fast and reliable design avoiding adhesive joints and overcoming the problems associated to end blocks and piano hinges. Additional details about the tool and how it functions can be followed in [19]. The device for the GDCB testing has been patented under the international publication number WO/2022/003219.

2. Data reduction methods

Taking into account that the signal of the load cell is not recommendable for high-rate tests, alternative load-independent analysis are required. Thus, three different data reduction methods have been defined for the analysis of the mode I fracture toughness using the GDCB test method proposed by Medina et al. [19].

2.1. Method 1: Displacement-based method with kinetic energy contribution

The first method formulation is based on the deductions of the first order beam theory described by Williams [20] and Hashemi et al. [21], and assuming the postulates of linear elastic fracture mechanics (LEFM). The detailed development of this method is described in [19]. Here, a brief summary of the method is presented here. For the case of the GDCB configuration of Fig. 2, where δ is the opening displacement at the loading point, P is the load with a transverse load equal to the axial-tensile load, $\dot{\delta}$ is the opening displacement rate, b is the width of the specimen, h is half of the specimen thickness, and a is the crack length; and making use of its compliance from Eq. (1), a displacement-based equation for the energy release rate can be obtained as in Eq. (2).

$$C = \frac{\delta}{P} \approx \frac{8a^3}{Ebh^3}\left(1 - \frac{3\delta}{5a}\right) \tag{1}$$

$$G_I = \frac{3Eh^3\delta^2}{16a^4}\left[\frac{\left(1 - \frac{\delta}{2a}\right)^2}{\left(1 - \frac{3\delta}{5a}\right)^2}\right] \tag{2}$$

where E is the flexural modulus of the laminate for an arbitrary stacking laminate, the axial modulus of the laminate for the case of unidirectional material or the modulus of the adherents for the case of an adhesively bonded joint.

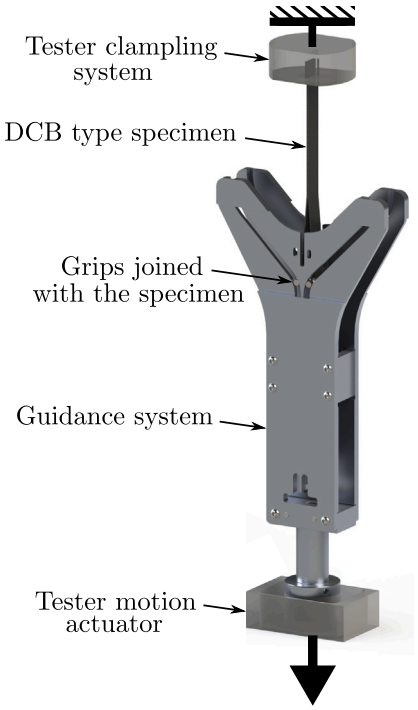

Fig. 1. GDCB tool for the different loading rates testing, from quasi-static to intermediate/high loading rates.

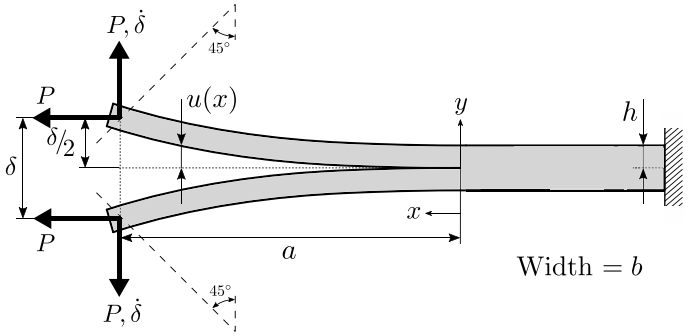

Fig. 2. Mode I guided double cantilever beam (GDCB) configuration.

Due to the existence of some deflection and rotation at the crack tip [21], the rotation of the arms at the crack tip is modelled by adding a length χh to the crack length, defining an effective crack length $a_e = a + \chi h$, where χ is a constant given by the elastic properties of the material as described in [21]. Then, the corrected expression for the mode I energy release rate using the GDCB method is:

$$G_{\mathrm{I}} = \frac{3Eh^3\delta^2}{16\left(a_e\right)^4}\left[\frac{\left(1-\frac{\delta}{2a_e}\right)^2}{\left(1-\frac{3\delta}{5a_e}\right)^2}\right] \tag{3}$$

Eq. (3) is useful when the contribution of the kinetic energy for the analysis of the mode I interlaminar fracture toughness is not relevant. This may occur in quasi-static cases and high-rate cases when the transition time threshold criterion proposed by Medina et al. [22] is fulfilled. However, in a high-rate scenario where the kinetic energy of the system might play an important role, its contribution to G_{I} can be calculated from the kinetic energy of a cantilever beam with a lumped mass m at the free end. Using simple beam theory and assuming the static displacement profile of a cantilever beam with a transverse loading, the kinetic energy

contribution can be expressed as:

$$U_{\mathrm{k}} = 2\left[\frac{1}{2}\int_0^a \rho b h\left[\dot{u}\left(\frac{3ax^2 - x^3}{2a^3}\right)\right]^2 \mathrm{d}x\right] + 2\left[\frac{1}{2}m\left(\dot{\delta}/2\right)^2\right] \tag{4}$$

$$\frac{\mathrm{d}U_{\mathrm{k}}}{\mathrm{d}a} = \frac{33\rho b h\dot{\delta}^2}{560} = \frac{33Ebh}{560}\left(\frac{\dot{\delta}}{c_{\mathrm{o}}}\right)^2 \tag{5}$$

where $c_{\mathrm{o}} = (E/\rho)^{1/2}$ is the longitudinal wave propagation velocity in the material and $\dot{\delta}$ is the opening loading rate. Finally, the displacement-based expression for the G_{I} of the GDCB method at high loading rates can be expressed as:

$$G_{\mathrm{I}} = \frac{3Eh^3\delta^2}{16\left(a_e\right)^4}\left[\frac{\left(1 - \frac{\delta}{2a_e}\right)^2}{\left(1 - \frac{3\delta}{5a_e}\right)^2}\right] - \frac{33Ebh}{560}\left(\frac{\dot{\delta}}{c_{\mathrm{o}}}\right)^2 \tag{6}$$

The displacement-based method has some limitations since it is based on a beam theory and LEFM. One of its limitations is that it depends on elastic properties that can be rate-sensitive for some materials. Moreover, measuring the crack length, which can be a complex task, has a huge effect on the accuracy of the method. In fact, this parameter appears to the fourth power in the expression and small measurement errors can lead to completely erroneous values of G_{Ic}. In addition, the contribution to the kinetic energy from the axial-loading present in the GDCB test method was not considered. Therefore, the dynamic contribution for the GDCB test, which corresponds to the last term in Eq. (6), has been assumed the same as for the DCB test. This assumption may be inaccurate at higher loading rates than the ones considered in this work.

2.2. Method 2: Crack tip local displacement method

For the second method, a data reduction method based on a near-crack-tip displacement formulation to obtain the mode I fracture toughness is proposed. In this method, the analysis must be focused as closely as possible to the crack tip, as shown in Fig. 3. The idea is to describe the behaviour of the experimental GDCB test by means of an equivalent DCB geometry case loaded with pure bending moments in the near-crack-tip region, carrying out a local analysis to determine the equivalent moments through the deformation of the arms in the near-crack-tip region. It is in this region where the formulation assumes a linear elastic behaviour of the specimen, thus, the inertia effects can be considered as negligible since the closer to the crack tip, the lower the mass considered and the lower the deformation of the arms due to dynamic effects. This allows the assumption that the dynamic GDCB problem can be treated as a quasi-static case of an equivalent DCB with pure bending moments close to the crack tip.

Performing the analysis in a near-crack-tip region, as illustrated in Fig. 3, the energy release rate of a DCB geometry under pure bending moments [23] can be described in terms of an equivalent moment M as:

$$G_{\mathrm{I}} = \frac{\varphi}{b}M^2 \tag{7}$$

where $\varphi^{-1} = EI = Ebh^3/12$, with I being the second moment of area of the cross section. Using the compliance of the DCB, a crack-dependent expression of the energy release rate can be defined as:

$$G_{\mathrm{I}} = \frac{3M\delta}{2ba^2} \tag{8}$$

In the expressions in Eqs. (7) and (8), the contribution of the axial-load of the GDCB is implicitly considered because it is based on a moment analysis and the equivalent moment is based on the experimental deformation of the arms near the crack tip.

Then, the equation for the energy release rate can be obtained using the Euler–Bernoulli theory where $M = \varphi^{-1}\mathrm{d}\phi/\mathrm{d}x$ and $\mathrm{d}\omega/\mathrm{d}x + \phi = 0$, $\omega(x)$ is the opening displacement of the arms near the crack tip and $\phi(x)$ the rotation of the arms near the crack tip, defined by the n-grade polynomial expressions:

$$\omega(x) = \omega_0 + \omega_1 x + \omega_2 x^2 + \omega_3 x^3 + \cdots + \omega_n x^n \tag{9}$$

$$\phi(x) = \phi_0 + \phi_1 x + \phi_2 x^2 + \phi_3 x^3 + \cdots + \phi_n x^n$$

For the case where the analysis is carried out sufficiently close to the crack tip, i.e., when $x \to 0$, the equivalent moment can be expressed as:

$$M = \varphi^{-1}\frac{\mathrm{d}\phi}{\mathrm{d}x} = \varphi^{-1}\phi_1 \tag{10}$$

This solution implies measuring the rotations close to the crack tip, which can require a complex set-up. However, measuring the near-crack-tip displacement profile can be performed in an easier and more accurate way than measuring the rotation profile when using high-speed cameras. Then, using the second derivative of the displacements of the arms, the equivalent moment can be expressed in terms only of the near-crack-tip displacement parameters as:

$$M = -\varphi^{-1}\frac{\mathrm{d}^2\omega}{\mathrm{d}x^2} = \varphi^{-1}(2\omega_2) \tag{11}$$

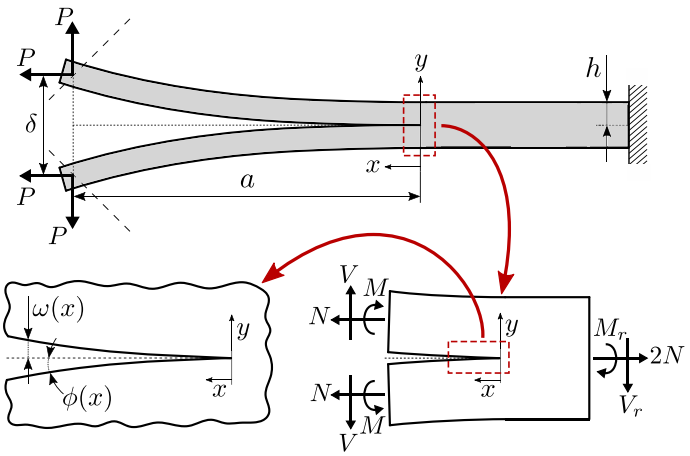

Fig. 3. GDCB configuration highlighting the near-crack-tip displacement profile $\omega(x)$ and rotation profile $\phi(x)$.

With this solution, the degree of the polynomial expression used for the description of the experimental displacement ($n \geq 2$) does not matter. However, when determining the opening displacement of the arms, for instance using an image analysis, it is important to define the correct grade of the polynomial fitting expression, since the coefficients can change drastically and the results may vary considerably. A third grade expression ($n = 3$) is chosen for this study since the quasi-static deformation of a cantilever beam is described by a third grade expression in beam theory [24].

The energy release rate in the GDCB can be determined by substituting the equivalent near-crack-tip moment from Eq. (11) in Eq. (8), resulting in what, from here on, will be referred to as the expression for Method 2a:

$$G_{\mathrm{I}} = \frac{3Eh^3\delta\omega_2}{12a^2} \tag{12}$$

Using Eq. (12) to determine the energy release rate has the advantage of reducing the fourth power of the crack length in Method 1 (Eq. (6)) to half of it (second power in (Eq. (12)). Thus, the possible errors associated with measuring the crack length should be reduced. However, the use of the second derivative of the near-crack-tip displacements represents a new source of errors.

Combining the displacement profile parameter in Eq. (11) with the alternative equation for the energy release rate in Eq. (7) results in the energy release rate expression for what from now on will be referred to Method 2b:

$$G_{\mathrm{I}} = \frac{Eh^3{\omega_2}^2}{3} \tag{13}$$

The use of Eq. (13) avoids the difficult task of physically measuring the crack length during the test. However, it still depends on the second derivative of the near-crack-tip displacements, which is the critical source of error.

This crack tip local displacement method still depends on the elastic properties that can be rate-sensitive for some materials. Moreover, the accuracy of the method relies on the accuracy of capturing the displacement profile close to the crack tip, thus a high resolution optical method (high speed cameras in this case) is required. Finally, the advantage of this method is that it can include the dynamic effects by using a quasi-static frame analysis. Since the method uses an equivalent cross-section internal moment around the crack tip in order to equilibrate the near-crack-tip displacements of the arms, this near-crack-tip loading state considers all the possible dynamic effects.

2.3. Method 3: Numerical-based method

The third method consists of a numerical assessment using the experimental displacement profiles of the arms in conjunction with the VCCT method [25] in a Finite Element (FE) model. In this method, the high-rate effects are captured by means of the displacement profile of the arms. However, in contrast to Method 2, the displacement profile for Method 3 considers a longer segment of the crack length.

In fact, the deformed shape of most of the length of the specimen arm is monitored or measured during the tests. In this way, not only the quasi-static deformation is captured, but so too is the deformation due to the dynamic and inertial effects. Although the deformed shapes of the two arms of the specimen should be symmetric, both arms are analysed to take into account that, due to inertial effects, small differences in the specimen arms can generate slightly different displacement profiles in each arm of the specimen during the test. Finally, a mean of the displacement profiles of both arms is obtained to be used as input for the FE analysis. Then, an FE simulation of the GDCB test is carried out imposing the mean experimental displacement profile. Applying the one evaluation step VCCT method (Fig. 4), the energy release rate can be obtained as:

$$G_{\mathrm{I}} = -\frac{1}{2\Delta a} R_y \Delta u_y \tag{14}$$

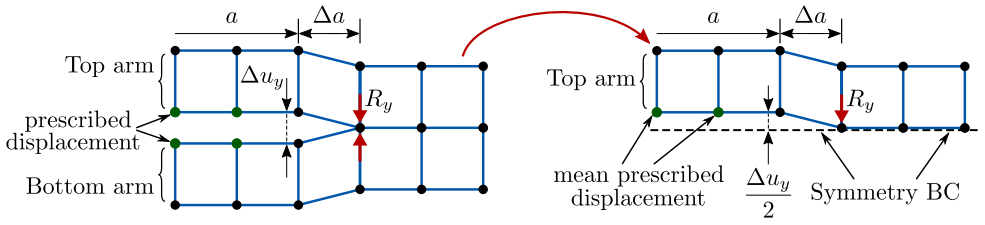

Fig. 4. Reaction force R_y and separation displacement Δu_y applied in VCCT analysis based on one evaluation step. Model considering both arms of the specimen in the left image and model considering symmetry of one arm in the right image.

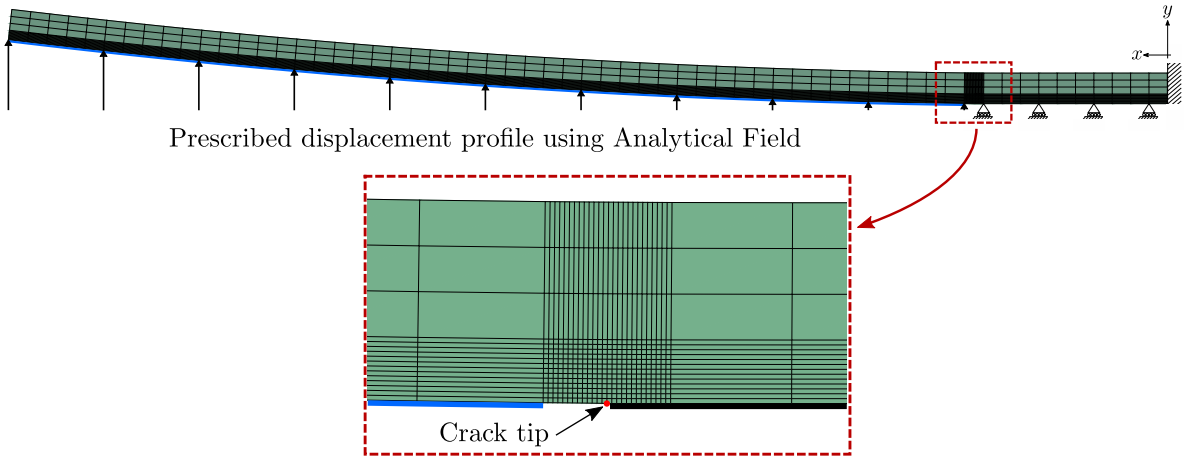

Fig. 5. Mesh and boundary conditions of the final model considering a segment of the full specimen length.

This method is a combination of experimental test data and numerical modelling, having the advantages of no-dependency on a beam theory, and less need for image accuracy to obtain the displacement profile in comparison with the data required for Method 2. However, the method has its limitations as the analysis is still based on LEFM and requires a large number of FE simulations. That said, computational costs and simulation times are relatively low.

For this study, a 2D linear elastic model using the commercial software Abaqus™/Standard [26] was developed. One half of the GDCB specimen (upper arm) was modelled and symmetric conditions were assumed, as shown in Fig. 5. The specimen was assumed to be unidirectional with all fibres parallel to the direction of the crack growth. The composite specimen was modelled using continuum elements with incompatible modes (CPS4I) which eliminate the shear locking phenomenon, properly capturing the bending behaviour [26]. The final mesh of the model was selected by carrying out a study with different mesh sizes looking for a good compromise between processing time and result accuracy. A unitary width size was used. A refined mesh of the model was used near the crack tip, as shown in Fig. 5, with an element size of 0.0385 mm in both directions. An element size of 0.95 mm was used along the length of the specimen for the coarse mesh region, an element size of 0.36 mm was defined in the through-thickness directions of the coarse mesh region.

The model of the segment of the GDCB had a crack length $a = 50$ mm, an arm thickness $h = 1.58$ mm, and a length $l = 60$ mm. The arm of the specimen was loaded imposing a prescribed displacement profile onto a segment of the crack length. This segment corresponds to the initial cracked length of 50 mm since it was the length used experimentally by the image post-processing to obtain the displacement profile of the arms. The displacement profile was obtained using a polynomial curve fitting of the images recorded during the tests. Then, the VCCT method was applied to obtain the value of the fracture toughness of the crack propagation for each prescribed displacement profile.

It is important to remark that this model using a segment of the full GDCB specimen was selected to reduce the computational time and the number of elements in the model. However, a comparison with a full GDCB specimen length model was performed to validate the results obtained with the reduced-length model. The full-length model was a 2D linear elastic model, as represented in Fig. 6. In this case, one half of the GDCB specimen (upper arm) was modelled and symmetric conditions were assumed, as was done for the model of the segment. The results of the fracture toughness obtained with the VCCT method were equal in both cases with less than 1% of difference, thus supporting the use of the segmented model.

A summary of the different methods proposed in this work for the data reduction of the GDCB test method is presented in Table 1.

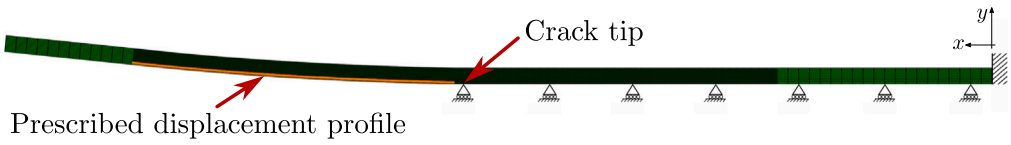

Fig. 6. Initial model for the full specimen length simulation.

Table 1
Summary of the data reduction method proposed for the GDCB test method.

Method	Expression for high-rates	Data inputs
1	$G_I = \frac{3Eh^3\delta^2}{16(a)^4}\left[\frac{\left(1-\frac{\delta}{2a}\right)^2}{\left(1-\frac{3\delta}{5a}\right)^2}\right] - \frac{33Ebh}{560}\left(\frac{\dot{\delta}}{c_o}\right)^2$	$\delta, \dot{\delta}, a$
2a	$G_I = \frac{3Eh^3\delta\omega_2}{12a^2}$	δ, a, ω_2
2b	$G_I = \frac{Eh^3{\omega_2}^2}{3}$	ω_2
3	$G_I = -\frac{1}{2\Delta a}R_y\Delta u_y$	$u(x)$

3. Materials and specimens

Two different materials were used in this study: a unidirectional Hexply® M21EV/34% /UD200/IMA/150ATL thermoset-matrix carbon fibre prepreg composite and an adhesively bonded joint made of an epoxy adhesive film FM® 300M with the previous carbon/epoxy composite as adherents. The properties of the materials used cannot be made public due to confidentiality. However, the elastic, strength and fracture properties of the materials are within the range of the materials commonly used in aeronautic applications.

A 16-ply plate with all layers oriented in the same direction was manufactured. The starter crack was introduced in the mid-plane with a non-adhesive polytetrafluoroethylene (Teflon) film. The laminate had a ply stacking sequence of $[0_8//0_8]$. The specimens' preparation was kept the same for the two test configurations, DCB and GDCB. The average specimen thickness was 3.165 mm for the carbon/epoxy composite material and 3.272 mm for the adhesively bonded joint with an adhesive thickness of around 0.1 mm. These thicknesses correspond to the mean value of cured specimens, counting six measures per specimen at different locations with a thickness variation within the limits established by the standard. The longitudinal edges of the specimens were polished with sandpaper of different grain sizes and coated with white spray paint to facilitate the optical tracking of the crack propagation.

The specimen geometry used for the GDCB test method is similar to the one defined for the ISO [5] DCB test method for the characterisation of the mode I interlaminar fracture toughness in laminated materials under quasi-static loading. However, the initial crack length and the total length of the specimen for the GDCB test are larger than the standard DCB specimen. These dimensions have been determined to ensure the initiation of propagation begins only once a constant opening velocity is reached during the propagation zone of the GDCB, as described in [19], without plastic deformation or failure in the arms of the specimen due to excessive bending or low stiffness. The in-plane dimensions of the GDCB samples were 350×20 mm^2. The pre-crack was 150 mm for both the composite laminate and the adhesively bonded joint. As recommended by the DCB standard [5], all pre-cracks were extended a few millimetres using the DCB set-up to avoid any influence of resin-rich pockets originated at the edge of the Teflon tape. Once the specimens were placed into the grips, the initial crack length was around 60 mm for the DCB and 146 mm for the GDCB. Four opening displacement rates were tested: quasi-static (QS), 1, 6 and 30 m/s. Four specimens per loading rate configuration were tested.

4. Testing set-up

The set-up was designed so that the different parameters needed for the data reduction methods could be obtained. As different reduction methods require different input parameters (see Table 1), a set of two cameras was used to obtain all of them at the same time for each test in order to assess the different methods employed in each test. As such, Method 1 and Method 2a require two cameras to obtain the different parameters, while Method 2b and Method 3 only require one camera to obtain their respective input parameters. For Method 1, the input parameters are the opening displacement at the loading point δ, the displacement rate at the loading point $\dot{\delta}$, and the crack length a. Method 2a requires the opening displacement at the loading point δ, the crack length a, and the near-crack-tip deformation parameter ω_2. Method 2b only needs the near-crack-tip deformation parameter, ω_2. Method 3 requires the deformation profile of the arms along a relatively long segment from the crack length $u(x)$. All of these were obtained during the tests using common reflex cameras for quasi-static tests and high-speed cameras for the high-rate tests; as will be described next.

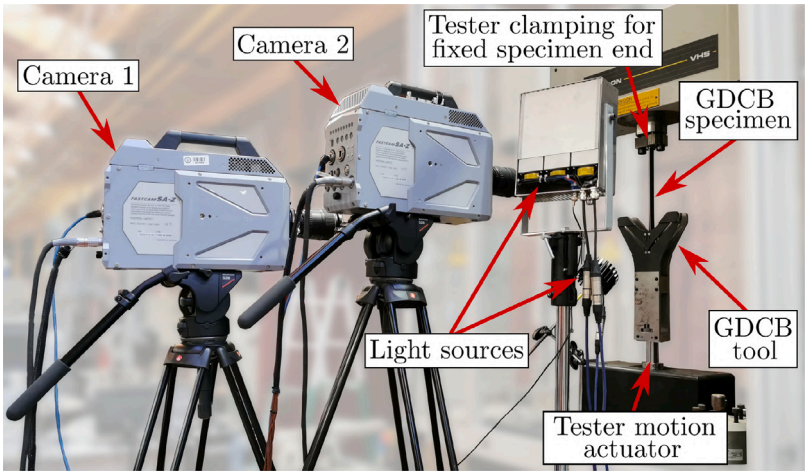

Fig. 7. GDCB set-up for high loading rate testing.

4.1. Quasi-static tests

The quasi-static tests were performed under controlled laboratory conditions using an electromechanical screw-driven MTS machine equipped with a 10 kN load cell for both the DCB and the GDCB, described in [19], test methods with a constant cross-head velocity of 5 mm/min. The DCB quasi-static tests were carried out according to the ISO [5] test method for the composite laminate and the ISO [6] test method for the adhesively bonded joint. The exception from the test standards was to use a Side-Clamped Beam (SCB) test fixture [27], and only four specimens were tested. According to the standards ISO 15024 and ISO 25217, the data reduction methods of the test were based on the Corrected Beam Theory (CBT).

In addition to the testing machine's own data acquisition system to record load and displacement, a set of two cameras was used for the GDCB QS tests: Camera 1 to track the grip pins and, depending on the data reduction method being used, Camera 2 to track different locations. Thus, Camera 2 is used to track the crack tip location for Method 1, the near-crack-tip displacement profile for Method 2, and the long range displacement profile for Method 3. The displacement at the load-application point was tracked optically by means of markers placed at the pins in the specimen grips. For the GDCB tests, the cameras recorded images at 0.2 Hz with a resolution of 2048 pixels along the loading direction and 328 pixels along the perpendicular direction for Camera 1, and 2048 × 2048 pixels for Camera 2. The lighting conditions during testing were set to provide a sharp contrast between the white specimen surface and the background.

4.2. Intermediate/high-rate tests

The intermediate/high displacement rate tests were carried out using the GDCB test method and an Instron VSH dynamic servo-hydraulic testing machine. The combination of this testing device and the GDCB test rig allows for a constant and symmetric opening displacement to be obtained independent of the loading rate of the test.

To reduce the experimental data and determine the energy release rate, the tests were monitored with a high-speed video system. The set-up, as shown in Fig. 7, consisted of a set of two cameras: Camera 1 to track the opening displacement at the load application points in the specimen for Method 1, and Camera 2 to monitor the crack length growth and the deformation profile of the specimen arms. This second camera captured data for the three methods. Two Photron Fastcam SA-Z high-speed cameras were used: Camera 1 with a Tokina 100 mm f/2.8 macro lens, a resolution of 896 × 544 pixels and a shutter speed of 1/61538 s; Camera 2 with a Pentax 100 mm f/4 macro lens, a resolution of 384 × 1024 and a shutter speed of 1/66667 s. Both cameras used a data acquisition rate of 42 000 fps for all the loading rates. A selected position signal on the machine was used to trigger the high-speed cameras system. The lighting conditions during testing were set to obtain a sharp contrast between the white specimen surface and the background using an in-house LED lighting system of more than 70 000 lumens [28].

4.3. Image post-processing

The image frames obtained from the quasi-static tests and the high-rate tests were post-processed using in-house Matlab scripts/algorithms to obtain the required data for each of the data reduction methods. The post-processing was the same for both the quasi-static and high-rate GDCB tests. Fig. 8 shows a photo frame for the set of two cameras used in the GDCB test. The photo frames from Camera 2 in Fig. 8b were rotated 90° anti-clockwise for the post-processing.

The script from Camera 1 analyses all the image frames to determine the current position of the grip pins and the reference markers. Then, the opening displacement is obtained as the distance between the two loading pins, as seen in Fig. 9. The reference

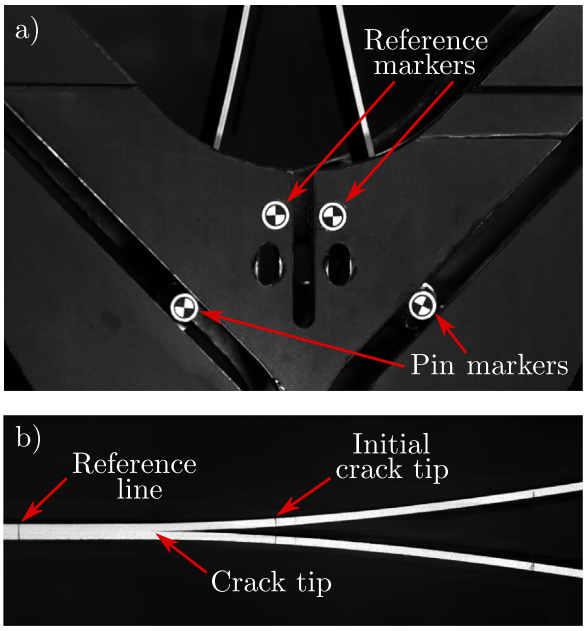

Fig. 8. Photo frames from (a) Camera 1 and (b) Camera 2 for the image post-processing of the GDCB.

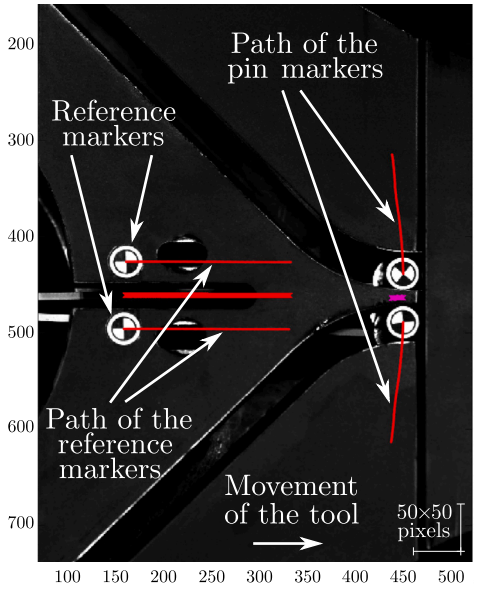

Fig. 9. Matlab script image from Camera 1 for the analysis of the GDCB (axes units in pixels).

markers are used as set points for the pin markers and as a control for the conversion from pixels to millimetres. Using the opening displacement and the test time, the opening loading rate can be calculated.

A second Matlab script was used to determine the current position of the crack tip and the arm displacement profiles during the test by post-processing the images taken with Camera 2. First, the displacement of the longitudinal outer edge of each specimen arm is detected and a polynomial expression is adjusted to each outer arm edge by a curve fitting process, as shown in Fig. 10a. Then, to obtain the crack length required as input data in Methods 1 and 2a, the edge points detected and the fitted curves are translated to the middle of the specimen where the crack is actually located, as shown in Fig. 10b. Finally, the crack tip is detected by the intersection of the two polynomial curves. It is important to mention that the outer edges of the specimen are used instead of the inner ones since an elastic behaviour with no shear effects is assumed and these surfaces are not affected by the waviness or small defects caused during the crack propagation, i.e., proving a clearer response.

Fig. 10. Matlab script images from Camera 2 for the analysis of the GDCB of (a) the outer edge detection, (b) translated edge curve fitting, (c) a zoom for the predicted crack for initial crack and (d) a zoom of an analysis during crack propagation.

The crack length obtained using this approach just before propagation starts is a bit longer than the crack length measured using the mark from specimen preparation with the predicted crack length, as seen in Fig. 10c. This difference is around 2 mm, which is similar to the values of the correction factor χh defined by Hashemi et al. [21] to determine an effective crack length. Therefore, this image post-processing approach already accounts for the rotation of the arms at the crack tip.

To determine the displacement profile parameter ω_2 for Methods 2a and 2b, the near-crack-tip portion of the initially detected outer edges of the specimen arms is used (Fig. 10(a). In this case, around half of the data points collected for the process to obtain the crack length are used, ensuring enough data points for the fitting process but being as close as possible to the crack tip to minimise the possible dynamic effects. Then, a third-grade polynomial expression is adjusted to each outer arm edge by a curve fitting process and the ω_2 parameter is determined. Finally, the polynomial expressions adjusted to the deflection of the specimen arms, as shown in Figs. 10b and 10d, are use to obtain the displacement profile $u(x)$, and therefore, to impose the prescribed displacements in the FE model used in Method 3.

5. Results and discussion

The results of the fracture toughness presented in this section have been normalised by the respective standardised quasi-static DCB value using the CBT data reduction method, $G_{\text{Ic-QS-CBT}}$. The results related to the composite laminate are presented first, followed by those for the adhesively bonded joint.

5.1. Opening loading rates

Fig. 11 summarises some examples of the evolution of the opening loading rates tested, 1, 6 and 30 m/s, and the corresponding displacement rate applied by the tester actuator for both material configurations, the composite laminate and the adhesively bonded

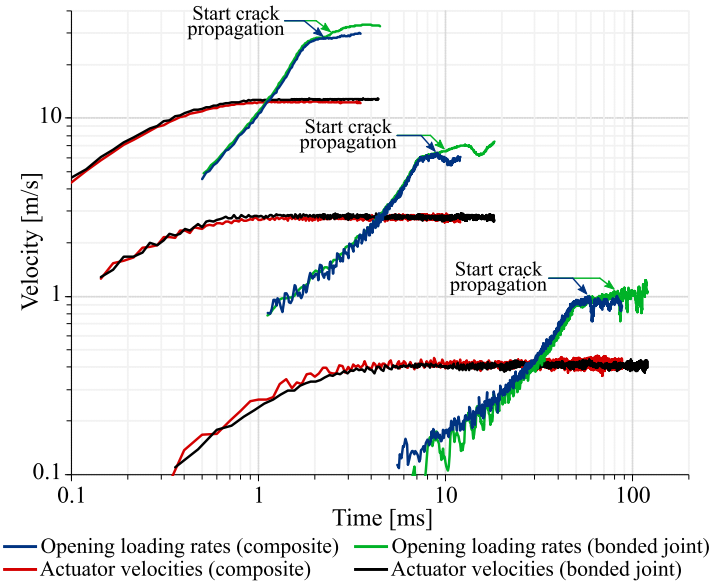

Fig. 11. Example of the opening loading rates achieved and the actuator velocities for the high-rate GDCB tests.

joint. The black and red curves show the acceleration ramp of the tester until reaching a constant velocity. The green and blue curves demonstrate that the crack opening of the specimens is happening when the actuator reached the predefined constant velocity. It is clear that the start of crack propagations is delayed in the case of the adhesively bonded joint. This can be due to the higher fracture toughness of the adhesive with respect to that of the composite, and the use of the same pre-crack length, which implies a higher deflection of the arms for crack propagation in the case of the adhesive. The curves also show some changes in the behaviour of the opening loading rates during the crack propagation, mainly because of the reduction in the stiffness of the arms when the crack increases.

5.2. Mode I fracture toughness: validation

The results of the mode I interlaminar fracture toughness of the composite material for the different loading rates tested are shown in Fig. 12. For the adhesively bonded joint, the results of the mode I fracture toughness for the different loading rates tested are shown in Fig. 13. First, these figures are used to compare the results obtained with the quasi-static GDCB (GDCB QS) and the DCB (DCB QS) test methods using the Method 1 data reduction procedure in both cases (Eq. (6) for the GDCB and its equivalent equation without the axial-load effect for the DCB). Analysing the DCB QS results from Fig. 12, these are slightly higher than those for the DCB QS-CBT. However, this is acceptable since the load-independent method can present some differences with respect to the CBT method because of how the data is collected and the simplifications introduced in the beam theory [29]. Comparing the GDCB QS and the DCB QS, the results can be considered as equivalent although the variability in the case of the GDCB is higher (Fig. 12b) and the mean value is closer to the unit ratio (Fig. 12a). Therefore, it can be considered that the GDCB testing method to characterise the mode I fracture toughness in composite materials has been validated. When analysing the intermediate/high-rate tests, at 1 m/s and 6 m/s, the results are below the reference values, i.e., the mean from Fig. 12a for each rate is out of the DCB QS-CBT range, but the corresponding dispersion (Fig. 12b) is higher and falls within the range of the quasi-static values. Analysing the tests at 6 m/s and 30 m/s, there is a clear increase in the dispersion of data, especially in the middle quartiles. For the case of 30 m/s, there is a low minimum value in the first quartile (Fig. 12b). In fact, during the experiments it was observed that at this loading rate the initiation values were always lower than those for the other loading rates. Despite this progressive increase in scatter, the resulting median values (Fig. 12a) are not sufficient to determine if there is a rate effect.

Regarding the analysis of Fig. 13 for bonded specimens, the DCB results are nearly equivalent to the DCB QS-CBT. When comparing the GDCB QS and the DCB QS, the results are similar. Both of them with a mean value below the QS-CBT one (Fig. 13a) and, with a higher dispersion in the case of the GDCB (Fig. 13b). This also validates the use of the GDCB test method for bonded joints. Moving to the high-rate tests, at 1 m/s the results are above the reference mean value but still in the range of the QS-CBT results. For 6 m/s, there is a decrease of the mean and an increase of the dispersion. Finally, for the case of 30 m/s, there is an increase of the dispersion of data (Fig. 13b), especially in the first quartile. This is because during the tests at 30 m/s, the initiation values of crack propagation were really low for this data reduction method. Although there is a higher scatter, the median values are in a range with those where no rate effect can be assumed.

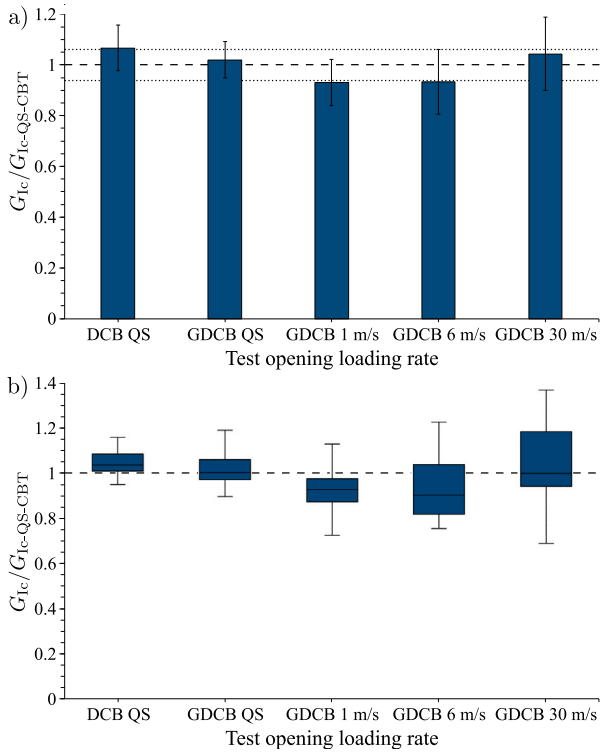

Fig. 12. Mode I interlaminar fracture toughness at different loading rates using Method 1 for the data reduction, showing (a) the mean and the standard deviation, and (b) the distribution of data.

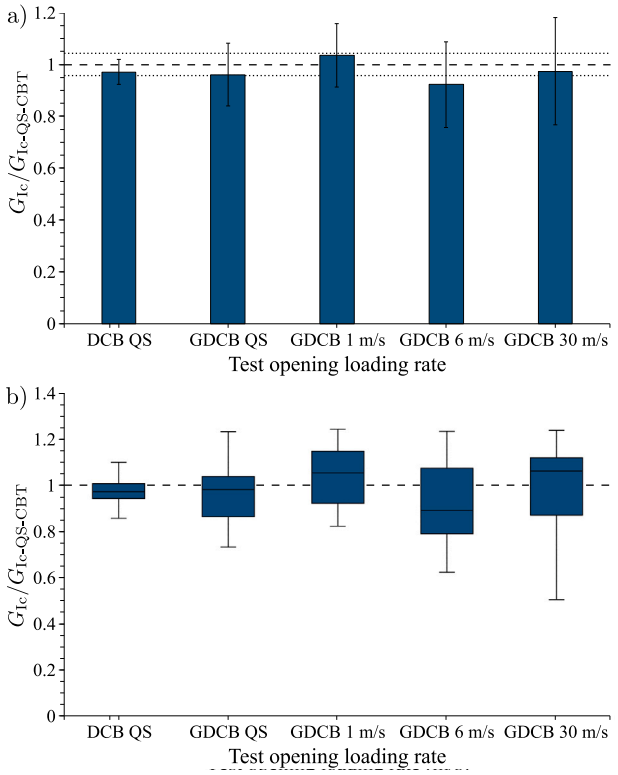

Fig. 13. Mode I adhesive fracture toughness at different loading rates using the Method 1 for the data reduction, showing in (a) the mean and the standard deviation, and in (b) the distribution of data.

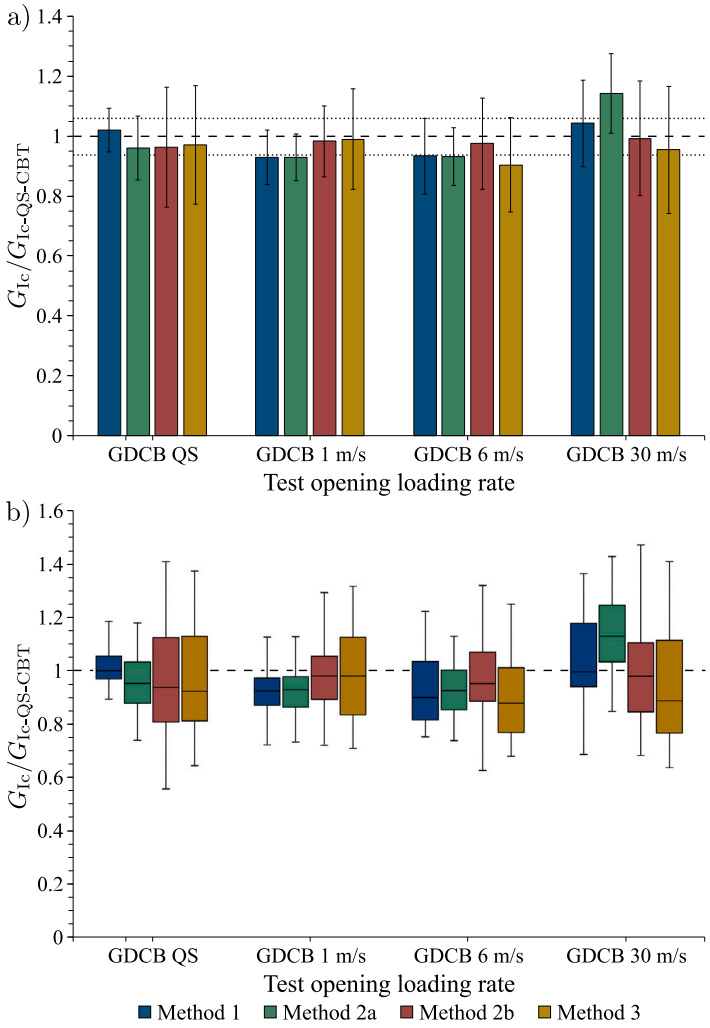

Fig. 14. Comparison of data reduction methods for mode I interlaminar fracture toughness at different loading rates, showing in (a) the mean and the standard deviation, and in b) the distribution of data.

5.3. Mode I fracture toughness: comparison of methods

A comparison of the different methods used for the data reduction of the GDCB tests with the composite material is presented in Fig. 14, and for the case of the adhesively bonded joint in Fig. 15. The results of the interlaminar fracture toughness from Fig. 14 determined with the four different data reduction methods are all similar and can be assumed as equivalent to the quasi-static ones. In the case of Methods 1 and 2a, there is a relatively large difference between values at different opening rates. Comparing the mean and the standard deviation of all the methods and velocities (Fig. 14a), it can be noticed that Methods 1 and 2a exhibit similar behaviour, with a decrease in the results for opening rates of 1 m/s and 6 m/s and an increase at 30 m/s when compared to the QS-CBT value. The results from Method 2b are similar for all the opening rates and close to the QS-CBT. In the case of Method 3, all the mean values are lower than the QS-CBT, with the lowest at 6 m/s. Although in general the results are close to the QS-CBT ones, there is no clear tendency in the variation of the results with the opening loading rate and data reduction method. This may be explained by the accuracy in the analysis of the images to obtain the data for the different data reduction methods. At high displacement rates, the resolution of the images is limited by the test set-up and the cameras being used, leading to a high dispersion in the results. Due to the scatter of the data, at this stage it cannot be clearly determined if the loading-rate has an effect on the fracture toughness of the material or not. Although the method and the set-up have been proven to be valid, additional tests with faster and higher resolution cameras are necessary.

When comparing the distribution of data for each method and velocity (Fig. 14b), while there is significant scatter in the data for some of the data reduction methods, similar trends can be observed for all cases. There is a tendency to increase the dispersion

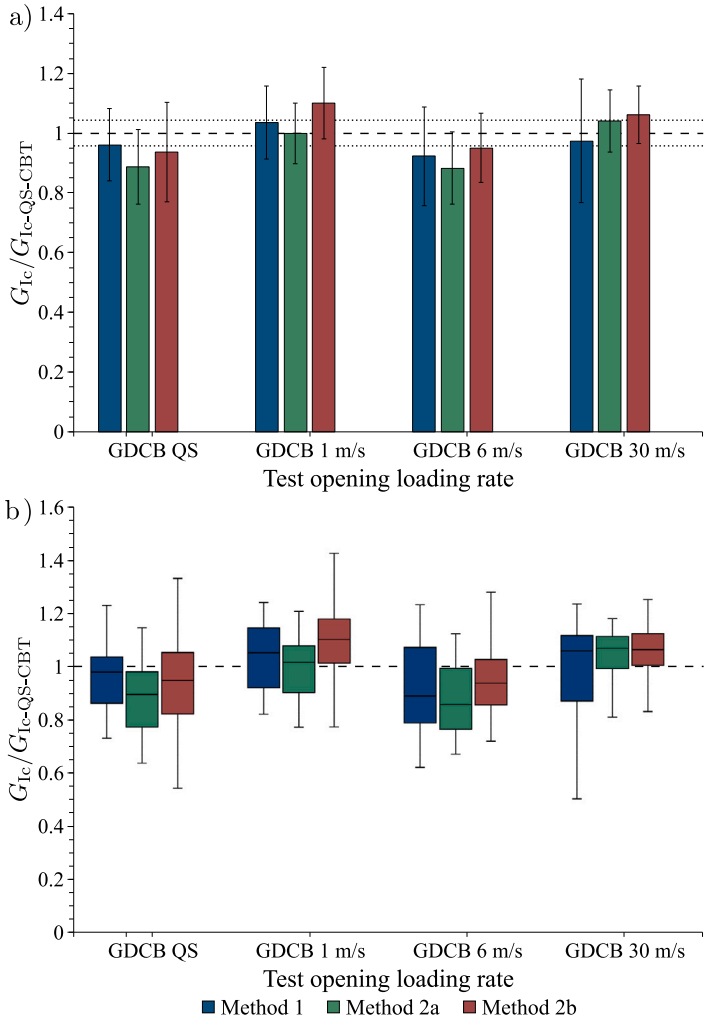

Fig. 15. Comparison of data reduction methods for mode I adhesive fracture toughness at different loading rates, showing in (a) the mean and the standard deviation, and in (b) the distribution of data.

with the increase of the opening loading rate for Methods 1 and 2a. However, Methods 2b and 3 present a high dispersion of data for all the opening rates. Additionally, it can be seen that the crack tip local displacement formulation of Method 2a is the one with the lesser dispersion, meanwhile the crack tip local displacement formulation of Method 2b is the one with higher dispersion in the results. This is linked to the accuracy in reading the input parameter for each of the data reduction methods. As explained earlier, and summarised in Table 1, Method 1 requires three input parameters of which two are associated to tracking at the loading point (opening displacement δ and opening velocity $\dot{\delta}$) and are captured directly from the image analysis with high accuracy. The remaining parameter, the crack length a, is accurately captured by the image post-processing script. This means that Method 1 has a low scattering in the results due to the accuracy of the input data. Method 2a also requires three input parameters of which two of them, the opening displacement δ and the crack length a, are captured as for Method 1, obtaining good accuracy. Meanwhile, the last parameter, the near-crack-tip displacement profile parameter ω_2, is not captured with that same high accuracy, promoting a higher scatter. However, since Method 2a involves two parameters captured with good accuracy and one parameter with low accuracy, the results obtained present low scatter. For the case of Method 2b, it depends on only one input parameter, the near-crack-tip displacement profile parameter ω_2, which presents low accuracy and results in the higher scattering in the results. Similarly, Method 3 requires the displacement profile $u(x)$ as input parameter, and as in the case of Method 2b, it is captured with low accuracy by the test set-up promoting a high dispersion of the results. As a conclusion, the dispersion in the results of the different data reduction method is linked not only with the parameters and the associated theory, but also with the accuracy of the set-up (resolution of the high speed cameras) and the post-processing used to capture the required input data. All these added to the inherent variability of the fracture toughness of composites.

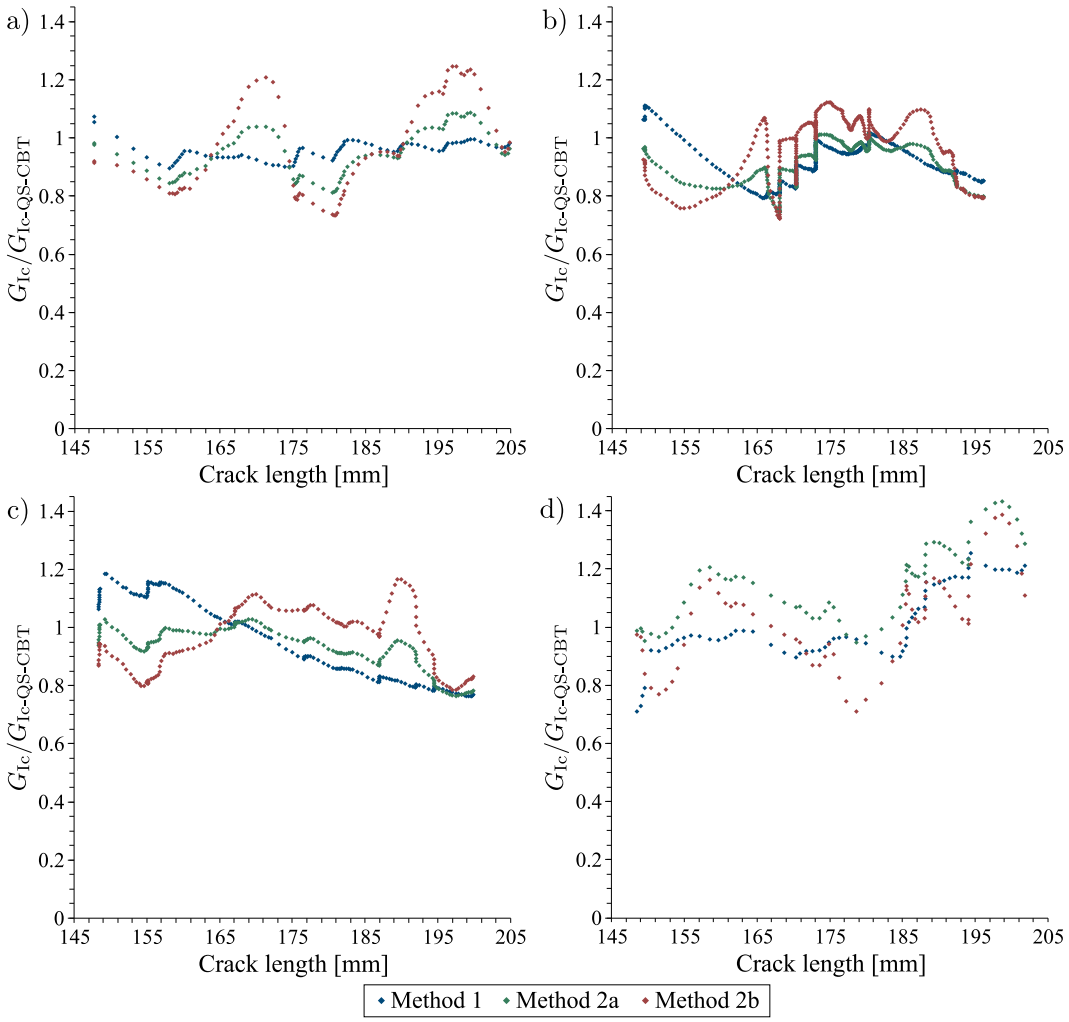

Fig. 16. Example of curves of the interlaminar fracture toughness in terms of the crack length for the composite laminate using three different data reduction methods for opening loading rates of (a) quasi-static, (b) 1 m/s, (c) 6 m/s, and (d) 30 m/s.

From Fig. 15, it is noticeable that for the case of adhesively bonded joint fracture toughness the results from Method 3 are not presented. This is because the FE model used for bonded joints is the same as for the case of the composite material (model described in Section 2.3), i.e., the model does not consider the physical adhesive layer or its properties. Applying the VCCT method to this model gave values of fracture toughness below half of the expected ones, indicating the need to improve the FE model, such as considering the adhesive layer and the corresponding material properties.

The results obtained using Method 1 are below the QS-CBT reference value at QS and 6 m/s, and 30 m/s loading rates. Method 2a presents the lowest mean values at QS and 6 m/s, and an increase of the fracture toughness with respect to the reference values for 30 m/s. For Method 2b, a similar behaviour to the results from Method 2a can be seen, with higher mean values in all cases. Method 2a always gives the lowest values while Method 2b corresponds to the highest ones except for the quasi-static case. In any case, as mentioned, the three methods result in similar fracture toughness values and fall within the variability range. For the case of 1 m/s opening displacement, the results are higher than the quasi-static values, but not enough to present a rate effect. Additionally, it can be observed that the dispersion in the results obtained with Method 1 tends to increase with the loading rate. On the contrary, the dispersion in the results for Method 2b is reduced with increasing loading rates. Method 2a presents a similar dispersion for all the cases.

Fig. 16 and Fig. 17 show a representative example of the curves of the interlaminar fracture toughness and the adhesive fracture toughness, respectively, in terms of the crack length for the tested loading rates using Method 1, Method 2a, and Method 2b for the data reduction. In Fig. 16, it can be seen how the curves of Method 2a tend to have a mean behaviour of the curves of Method 1 and Method 2b, confirming the explanation given before about the influence the parameters have on the dispersion of the results. Additionally, it can be noticed that at high loading rates, i.e., at 30 m/s, the fracture toughness starts with low values and increases

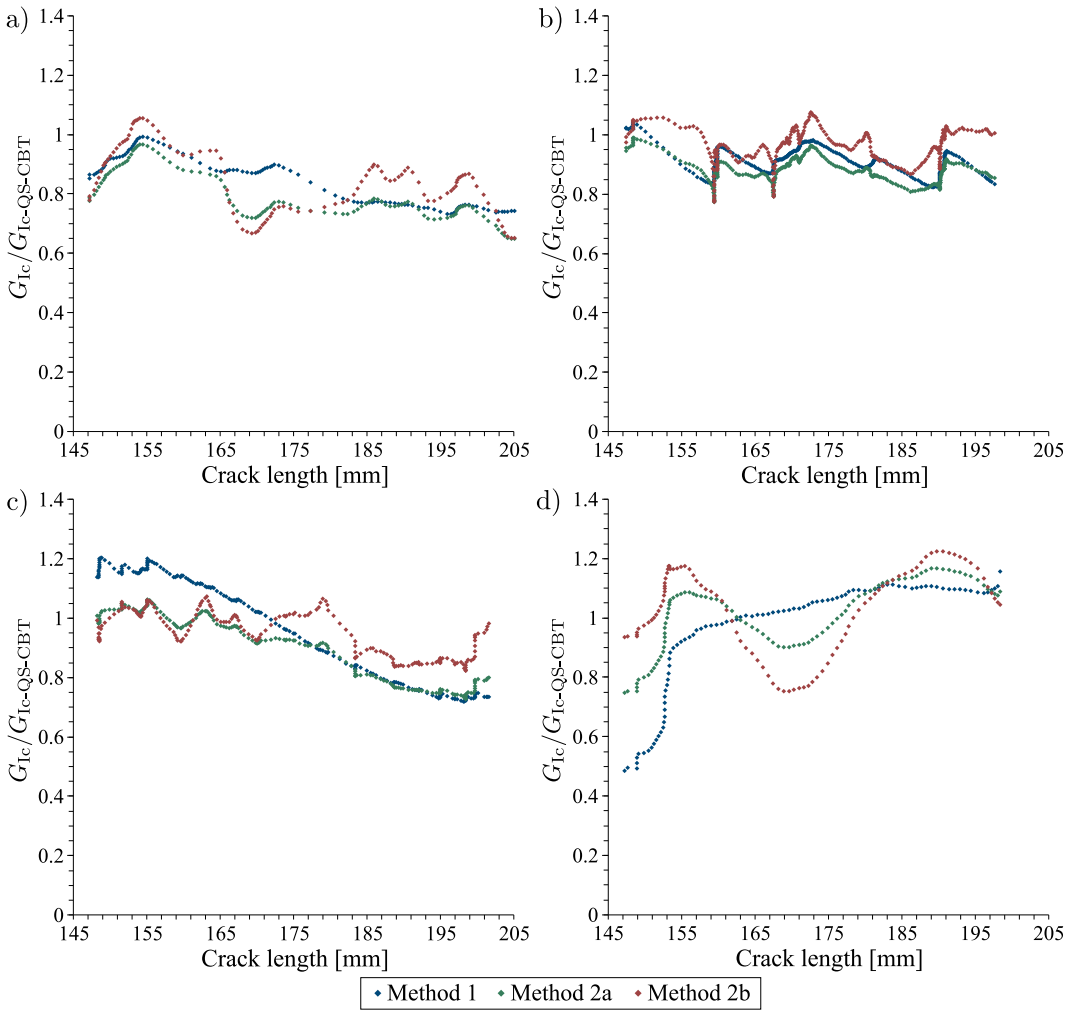

Fig. 17. Example of curves of the adhesive fracture energy in terms of the crack length for the bonded joint using three different data reduction methods for opening loading rates of (a) quasi-static, (b) 1 m/s, (c) 6 m/s, and (d) 30 m/s.

with the crack propagation, thus having a wide range of data and therefore a high dispersion. This behaviour can be due to the increase on the inertia effects linked to the large deformation of the arms.

Similar to the case for the composite laminate, the curves of Method 2a tend to present a mean behaviour of the curves of Method 1 and Method 2b in Fig. 17 for the adhesive joint. Besides, as in the case of the composite material, the behaviour of the fracture toughness for the adhesive joint with a low initial value at high opening rates (30 m/s) when using Method 1 can be seen. However, this behaviour is not noticed for the other two data reduction methods, dealing in a better way with the inertia effects at high loading rates.

In addition, the failure surfaces of all tested specimens were visually inspected after the tests. Fig. 18 and Fig. 19 present a representative example of the failure surfaces for the composite material and the bonded joint, respectively, at the different loading rates tested. It can be observed that for all cases it is possible to notice the signs of the pre-cracking process. However, from Fig. 18, there is no perceptible difference in the fracture mechanism between the different loading rates, obtaining stable and smooth crack propagation along the interface of the composite laminate. From Fig. 19 for the adhesive QS specimens, the final crack propagation mark was easily observed. This is because the test ends at a controlled crack extension, while for the intermediate/high loading rates, the test ends after a crack extension of around 150 mm. In general, stable and smooth crack propagation along the adhesive bond was obtained for all cases. A decrease of the possible arrest lines is noticed when increasing the loading rate. A cohesive failure that stays within the bondline for all the cases, from QS to high loading rates, was obtained.

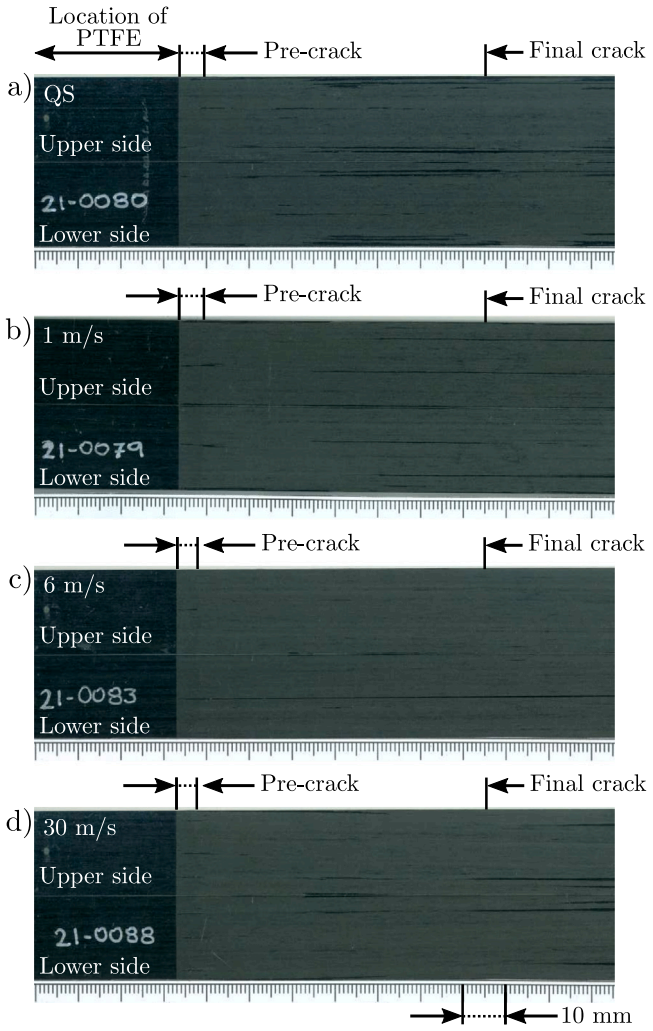

Fig. 18. Example of the main section of the cracked surfaces of the GDCB test for the composite laminate at (a) QS, (b) 1 m/s, (c) 6 m/s, and (d) 30 m/s loading rate.

5.4. Mode I fracture toughness: crack propagation velocity

Fig. 20 and Fig. 21 summarise the results of the interlaminar fracture toughness for the composite material and the adhesively bonded join, respectively, for each of the loading rates in terms of the crack propagation velocities. These figures are obtained by considering the mean value of the fracture toughness and the associated standard deviation for different values of crack propagation velocities for each tester loading rate. In addition, the density distribution for the crack velocities for the tested loading rates, shown in Fig. 20a and Fig. 21a, is included to give an idea of the relationship between the testing opening loading rate and the crack propagation velocities associated. Only the data reduction Methods 1, 2a and 2b are used mainly because Method 3 does not capture the crack length, thus, a crack propagation velocity cannot be assessed. Actually, Method 2b is crack length independent, presenting a similar case as Method 3, however the crack length data from Method 2a is used for Method 2b.

As shown in Fig. 20, a wide range of crack propagation velocities can be achieved for each one of the tester loading rates. For the tester loading rate of 1 m/s, crack propagation velocities between 0.05 m/s and 8.5 m/s were reached, thus having the main range of data between 1.5 and 4 m/s. For the tester loading rate of 6 m/s between 0.25 m/s and 40 m/s of crack propagation velocity, with the main range of data being between 10 and 30 m/s. For the tester loading rate of 30 m/s between 4.5 m/s and 70 m/s, with the main range of data being between 25 and 55 m/s. Therefore, the higher the tester loading rate, the lower the ratio between the crack propagation velocity and the loading rate. In addition, despite the scatter of the fracture toughness in Fig. 20a, b, and c, the mean values are similar for the different data reduction methods. It is possible to conclude that for these loading rates, there is no apparent effect on the fracture toughness of the composite material. Thus, when comparing the three different methods in Fig. 20, Method 2b seems to be the one that better eliminates the uncertainties at high loading rates.

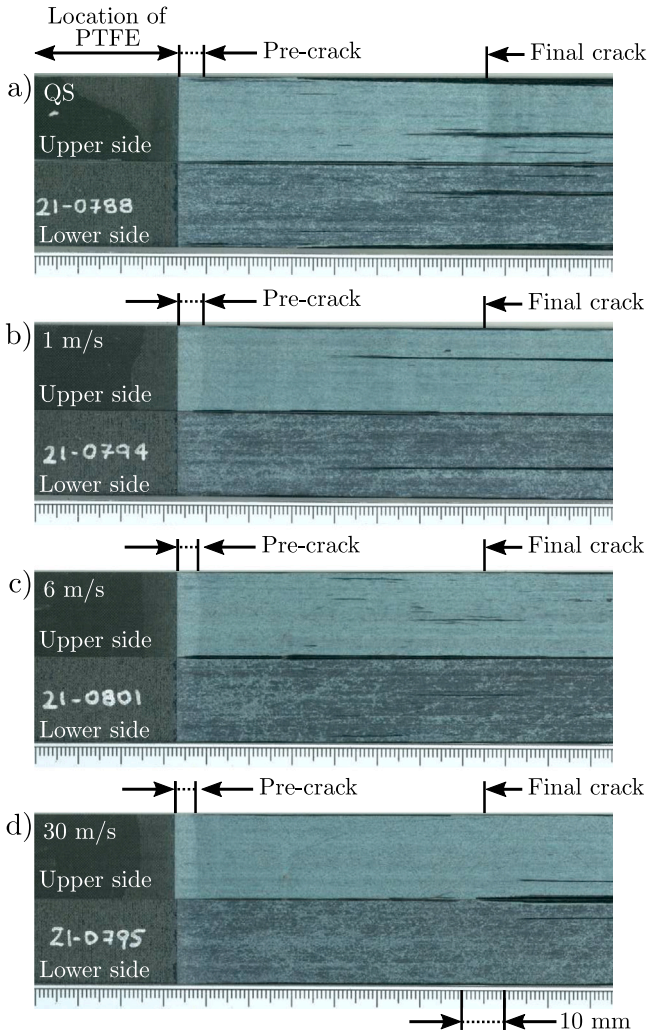

Fig. 19. Example of the main section of the cracked surfaces of the GDCB test for the adhesively bonded joint at (a) QS, (b) 1 m/s, (c) 6 m/s, and (d) 30 m/s loading rate.

Analysing Fig. 21, for the loading rate of 1 m/s, crack propagation velocities between 0.07 m/s and 5 m/s were reached, with the main range of data being between 1 and 3 m/s. For the loading rate of 6 m/s, the resulting crack propagation velocities are between 0.08 m/s and 20 m/s, with the main range of data being between 9 and 20 m/s. For the loading rate of 30 m/s, the crack propagation velocities found are between 1.5 m/s and 50 m/s, with the main range of data being between 15 and 40 m/s. In a similar case as the composite laminate, the higher the loading rate the lower the ratio between the crack propagation velocity and the loading rate. However, lower crack propagation velocities were reached in the bonded joint when compared to the composite laminate. Taking this into account, it is possible to conclude that the propagation velocity of the crack is slower in the adhesive used.

Overall, the fracture toughness results shown in Fig. 21 for adhesively bonded joint specimens present a similar dispersion. For the results using Method 1 (Fig. 21a), there seems to be a tendency of decreasing the fracture toughness with the crack propagation velocity and the opening loading rate. However, the low values of the fracture toughness at low crack propagation velocities for the loading rate of 30 m/s can be explained by the low initiation values that are usually at the lower crack propagation velocities, as seen in Fig. 17d. In addition, for the adhesive bonded joint tests, the loading rate of 6 m/s produces lower results for the three different data reduction methods. Therefore, despite the resulting scatter, it is not possible to conclude if there is an effect of the loading rates considered on the adhesive fracture toughness.

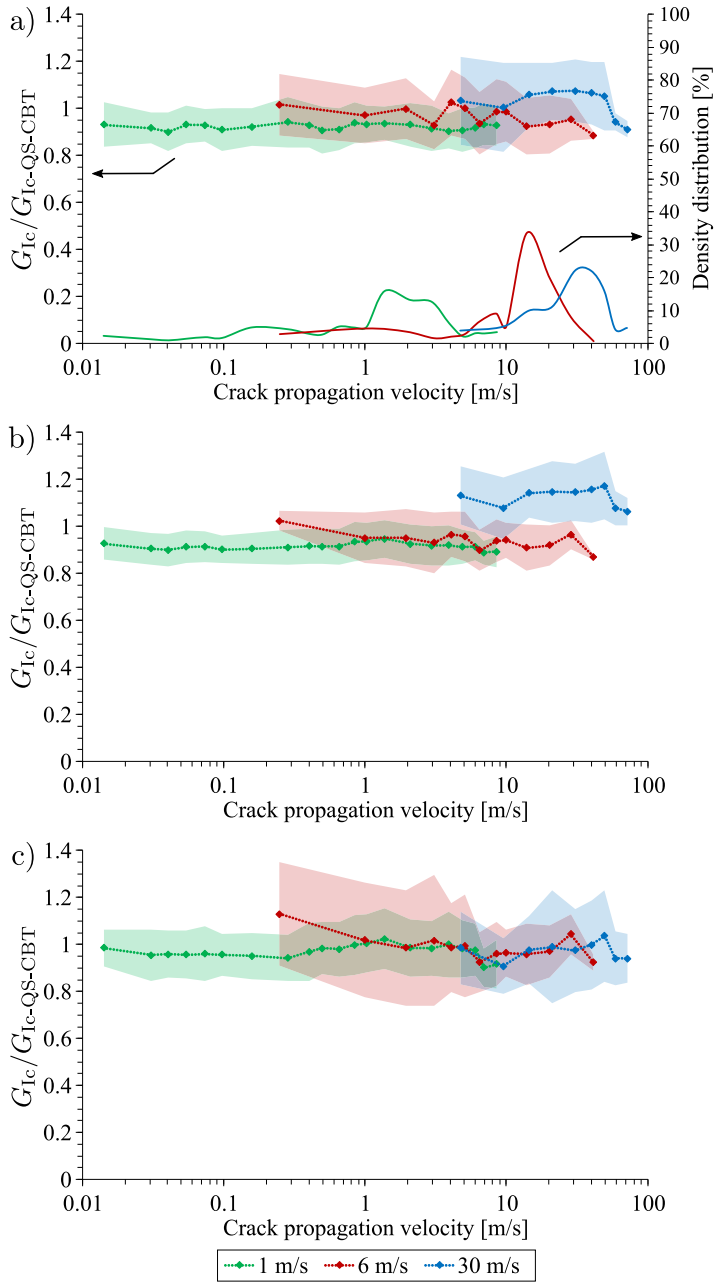

Fig. 20. Interlaminar fracture toughness in terms of the crack propagation velocities and the density distribution for the composite laminate using (a) Method 1, (b) Method 2a, and (c) Method 2b. Graph (a) also shows the density distribution of data which applies for the three different methods.

6. Conclusions

The rate-dependencies of the mode-I fracture toughness in a thermoset-matrix carbon-fibre composite and an adhesively bonded joint were assessed. Three different data reduction methods have been developed and compared. The study comparing the three different methods has been performed at different loading rates (from quasi-static to high-rate). In general, the results of the methods presented show a similar overall behaviour, but with clear differences in scattering. The results show no rate-dependency on the mode I fracture toughness higher than the uncertainty for the materials and the loading rates considered. A larger specimen sample per configuration could help to study the variability of the results and obtain a more reliable conclusion about the loading rate effect on the mode I fracture toughness.

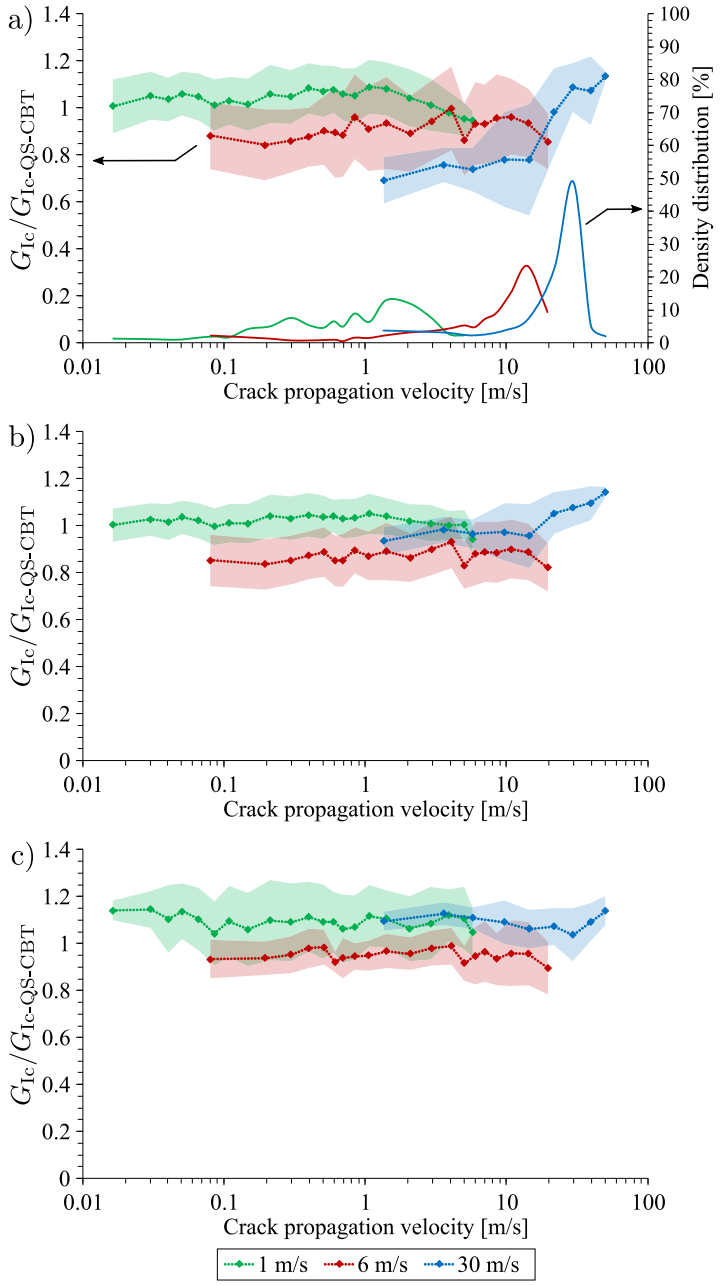

Fig. 21. Adhesive fracture toughness in terms of the crack propagation velocities and the data distribution for the bonded joint using (a) Method 1, (b) Method 2a, and (c) Method 2b. Graph (a) also shows the density distribution of data which applies for the three different methods.

Method 2a, based on the opening displacement, the crack length and the displacement profile parameter near the crack tip, is the one that presents lower scattering in the results. Meanwhile, Method 2b, which is only based on the displacement profile parameter near the crack tip, is the one that has higher dispersion. The numerically-based method (Method 3), which requires the displacement profiles of the arms, shows a similar scattering as Method 2b for the case of the composite laminate. Therefore, the methods dependent on the displacement profile, Method 2b and Method 3, can be improved by increasing the resolution of the image acquisition system. Method 2b is a promising data reduction method for dynamic testing because it only requires a single high-speed camera. Even though the experimental variability, the dynamic mean values lie within the range of the G_{Ic} measured with the QS DCB.

Finally, a better pre-crack length for the adhesively bonded joints must be used instead of using the same crack as the one defined for the composite fracture toughness specimens.

CRediT authorship contribution statement

S.A. Medina: Writing – original draft, Software, Methodology, Investigation, Formal analysis, Conceptualization. **E.V. González:** Writing – review & editing, Supervision, Conceptualization. **N. Blanco:** Writing – review & editing, Supervision, Conceptualization. **P. Maimí:** Writing – review & editing, Conceptualization. **J. Pernas-Sánchez:** Writing – review & editing, Resources, Investigation. **J.A. Artero-Guerrero:** Writing – review & editing, Resources, Investigation. **P. Hahn:** Methodology, Investigation. **M. May:** Writing – review & editing, Resources, Investigation. **E. de Blanpré:** Supervision, Resources. **V. Jacques:** Supervision, Resources.

Declaration of competing interest

The authors declare the following financial interests/personal relationships which may be considered as potential competing interests: S.A. Medina reports financial support was provided by Spain Ministry of Science and Innovation. E.V. Gonzalez reports financial support was provided by Clean Sky 2 Joint Undertaking.

Data availability

Data will be made available on request.

Acknowledgments

This project has received funding from the Clean Sky 2 Joint Undertaking (JU) under grant agreement No. 886519. The JU receives support from the European Union's Horizon 2020 research and innovation programme and the Clean Sky 2 JU members other than the Union. The first author acknowledges the grant for doctoral studies IFUdG2017/43 and the financial support from the Spanish Ministerio de Ciencia, Innovación y Universidades through the project RTI2018-099373-B-100.

References

[1] Blackman BRK, Kinloch AJ, Wang Y, Williams JG. The failure of fibre composites and adhesively bonded fibre composites under high rates of test. Part II Mode I loading - dynamic effects. J Mater Sci 1996;31(17):4451–66. http://dx.doi.org/10.1007/BF00366341.
[2] May M. Measuring the rate-dependent mode I fracture toughness of composites – A review. Composites A 2016;81:1–12. http://dx.doi.org/10.1016/j.compositesa.2015.10.033.
[3] Körber H. Mechanical response of advanced composites under high strain rates [Ph.D. thesis], Faculdade de Engenharia - Universidade do Porto; 2010.
[4] Neumayer J, Kuhn P, Koerber H, Hinterhölzl R. Experimental determination of the tensile and shear behaviour of adhesives under impact loading. J Adhes 2016;92(7–9):503–16. http://dx.doi.org/10.1080/00218464.2015.1092387.
[5] ISO 15024:2001. Fibre-reinforced plastic composites — Determination of mode I interlaminar fracture toughness, GIC, for unidirectionally reinforced materials. Geneva, CH: International Standardization Organization; 2001, p. 24.
[6] ISO 25217:2009. Adhesives — Determination of the mode I adhesive fracture energy of structural adhesive joints using double cantilever beam and tapered double cantilever beam specimens. Geneva, CH: International Standardization Organization; 2009, p. 24.
[7] Blackman BRK, Dear JP, Kinloch AJ, Macgillivray H, Wang Y, Williams JG, et al. The failure of fibre composites and adhesively bonded fibre composites under high rates of test. Part I Mode I loading - experimental studies. J Mater Sci 1995;30(23):5885–900. http://dx.doi.org/10.1007/BF01151502.
[8] Blackman BRK, Kinloch AJ, Rodriguez Sanchez FS, Teo WS, Williams JG. The fracture behaviour of structural adhesives under high rates of testing. Eng Fract Mech 2009;76(18):2868–89. http://dx.doi.org/10.1016/j.engfracmech.2009.07.013.
[9] Colin de Verdiere M, Skordos AA, May M, Walton AC. Influence of loading rate on the delamination response of untufted and tufted carbon epoxy non crimp fabric composites: Mode I. Eng Fract Mech 2012;96:11–25. http://dx.doi.org/10.1016/j.engfracmech.2012.05.015.
[10] Dillard DA, Pohlit DJ, Jacob GC, Starbuck JM, Kapania RK. On the use of a driven wedge test to acquire dynamic fracture energies of bonded beam specimens. J Adhes 2011;87(4):395–423. http://dx.doi.org/10.1080/00218464.2011.562125.
[11] Xu S, Dillard D. Determining the impact resistance of electrically conductive adhesives using a falling wedge test. IEEE Trans Compon Packag Technol 2003;26(3):554–62. http://dx.doi.org/10.1109/tcapt.2003.817646.
[12] Simon JC. Response and failure of adhesively bonded automotive composite structures under impact loads [Master of science thesis], Virginia Tech; 2004.
[13] Pohlit DJ. Dynamic mixed-mode fracture of bonded composite joints for automotive crashworthiness [Master of science thesis], Virginia Tech; 2007.
[14] Yamagata Y, Lu X, Sekiguchi Y, Sato C. Experimental investigation of mode I fracture energy of adhesively bonded joints under impact loading conditions. Appl Adhes Sci 2017;5(1):7. http://dx.doi.org/10.1186/s40563-017-0087-7.
[15] Isakov M, May M, Hahn P, Paul H, Nishi M. Fracture toughness measurement without force data – Application to high rate DCB on CFRP. Composites A 2019;119:176–87. http://dx.doi.org/10.1016/j.compositesa.2019.01.030.
[16] Thorsson SI, Waas AM, Schaefer J, Justusson B, Liguore S. Effects of elevated loading rates on mode I fracture of composite laminates using a modified wedge-insert fracture method. Compos Sci Technol 2018;156:39–47. http://dx.doi.org/10.1016/j.compscitech.2017.12.018.
[17] Riezzo M, Simmons M, Russell B, Sket F, nez VM, González C. Dynamic characterisation of interlaminar fracture toughness in carbon fibre epoxy composite laminates. Composites A 2019;126:105597. http://dx.doi.org/10.1016/j.compositesa.2019.105597.
[18] Lißner M, Alabort E, Erice B, Cui H, Blackman B, Petrinic N. On the dynamic response of adhesively bonded structures. Int J Impact Eng 2020;138:103479. http://dx.doi.org/10.1016/j.ijimpeng.2019.103479.
[19] Medina S, González E, Blanco N, Pernas-Sánchez J, Artero-Guerrero J. Guided double cantilever beam test method for intermediate and high loading rates in composites. Int J Solids Struct 2023;264:112118. http://dx.doi.org/10.1016/j.ijsolstr.2023.112118.
[20] Williams JG. On the calculation of energy release rates for cracked laminates. Int J Fract 1988;36(2):101–19. http://dx.doi.org/10.1007/BF00017790.
[21] Hashemi S, Kinloch AJ, Williams JG. The analysis of interlaminar fracture in uniaxial fibre-polymer composites. Proc. R. Soc. Lond. Ser. A Math. Phys. Eng. Sci. 1990;427(1872):173–99.
[22] Medina S, González E, Blanco N. Transition time threshold for Double Cantilever Beam specimens under high loading rates. Eng Fract Mech 2021;249:107754. http://dx.doi.org/10.1016/j.engfracmech.2021.107754.
[23] Freiman SW, Mulville DR, Mast PW. Crack propagation studies in brittle materials. J Mater Sci 1973;8(11):1527–33. http://dx.doi.org/10.1007/BF00754886.

[24] Berry JP. Some kinetic considerations of the Griffith criterion for fracture—I: Equations of motion at constant force. J Mech Phys Solids 1960;8(3):194–206. http://dx.doi.org/10.1016/0022-5096(60)90038-7.
[25] Rybicki E, Kanninen M. A finite element calculation of stress intensity factors by a modified crack closure integral. Eng Fract Mech 1977;9(4):931–8. http://dx.doi.org/10.1016/0013-7944(77)90013-3.
[26] Dassault Systèmes Simulia Corp. Abaqus Analysis User's Manual. In: Abaqus documentation 6.14. Providence, RI, USA: Simulia Worldwide Headquarters; 2014.
[27] Renart J, Blanco N, Pajares E, Costa J, Lazcano S, Santacruz G. Side Clamped Beam (SCB) hinge system for delamination tests in beam-type composite specimens. Compos Sci Technol 2011;71(8):1023–9. http://dx.doi.org/10.1016/j.compscitech.2010.10.005.
[28] Artero-Guerrero J, Pernas-Sánchez J, López-Puente J, Varas D. Experimental study of the impactor mass effect on the low velocity impact of carbon/epoxy woven laminates. Compos Struct 2015;133:774–81. http://dx.doi.org/10.1016/j.compstruct.2015.08.027.
[29] Xu W, Guo Z. A simple method for determining the mode I interlaminar fracture toughness of composite without measuring the growing crack length. Eng Fract Mech 2018;191:476–85. http://dx.doi.org/10.1016/j.engfracmech.2018.01.014.